



CALCULATION OF THE 1D LITHOFACIES DISCRIMINATION ATTRIBUTE DRIVEN BY ROCK PHYSICS MODELLING OF MAASTRICHTIAN RESERVOIRS FROM THE HIGH BLOCK OF THE RONCADOR FIELD, CAMPOS BASIN

Mario Florencio Barreto Paiva ^{1,2*} and Wagner Moreira Lupinacci ^{1,2}

ABSTRACT. The use of impedances derived from seismic and well data is a powerful methodology aiming geophysical reservoir characterization. However, impedance calculation often lacks geological information, being up to the interpreter associate it with the computational and physical parametrizations behind the inversion process. This scenario may lead to ambiguous or even erroneous interpretations. Thus, we propose an approach of Elasto-Facies Association (EFA) driven by rock physics modelling, in an attempt to bring more geological correlation in comparison with other widely used techniques (probabilistic, unsupervised or neural networks). This analysis is based on depth trends for P-wave velocity, which, for this case, clearly revealed the dependence of elastic properties on diagenetic effects as grain sorting, cementation and mechanical compaction. Thus, we investigated how these effects impact on seismic amplitudes and elastic impedances and their correlation with petrophysical properties for reservoir and non-reservoir rocks of intervals of interest. Finally, we applied the AVOImpedance technique (AVOI), creating a new attribute based on the projection of Acoustic Impedance (AI) and Elastic Impedance (EI2), named Lithological Discrimination Attribute (LDA). It was successful in characterizing the main lithological clustering and properly discriminating the Elasto-Facies for Maastrichtian reservoirs from the High Block of the Roncador Field.

Keywords: AVO analysis, seismic inversion, rock physics, reflection coefficient modelling, elastic impedance analysis.

RESUMO. A utilização das impedâncias derivadas dos dados sísmicos e de poços gera um importante conjunto de informações que auxilia na caracterização geofísica do reservatório. Entretanto, o cálculo das impedâncias carece de integração com as informações geológicas, sendo responsabilidade do intérprete associá-las às parametrizações computacionais do algoritmo de inversão. Isso pode frequentemente produzir resultados ambíguos ou erro nas interpretações. Assim, nós propomos um estudo das Elasto-Fácies Associadas (EFA), baseado em modelos de física de rochas, atribuindo assim um modelo mais geológico do que outras técnicas largamente utilizadas (probabilística, não-supervisionada ou redes neurais). Essa análise é baseada nas tendências das velocidades de onda-P com a profundidade, o que revelou uma estreita dependência com os efeitos diagenéticos, como seleção, cimentação e compactação mecânica. A partir dessa constatação, investigamos como esses efeitos influenciam as amplitudes sísmicas, impedâncias e propriedades petrofísicas das rochas reservatório e não-reservatório dos intervalos de interesse. Por fim, aplicamos a técnica de Impedância de AVO (AVOI) gerando um atributo, baseado na projeção das impedâncias acústica (AI) e elástica (EI2), chamado Atributo de Discriminação de Litofácies (LDA). Ele obteve sucesso na caracterização dos principais agrupamentos litológicos e discriminou adequadamente as Elasto-Fácies para reservatórios Maastrichtianos do Bloco Alto do Campo de Roncador.

Palavras-chave: análise de AVO, inversão sísmica, física de rochas, modelagem dos coeficientes de reflexão, análise das impedâncias elásticas.

*Corresponding author: Mario Florencio Barreto Paiva

¹Universidade Federal Fluminense - UFF, Exploratory Interpretation and Reservoir Characterization Group (GIECAR), Department of Geology and Geophysics, Niterói, RJ, Brazil – E-mail: wagnerlupinacci@id.uff.br

²Schlumberger Serviços de Petróleo Ltda. – E-mail: mfbp1979@gmail.com

³National Institute of Science and Technology of Petroleum Geophysics (INCT-GP/CNPq), Niterói, RJ, Brazil

INTRODUCTION

The use of elastic attributes is common in the oil industry and its beginning dates appear in the 1980s with the work of Aki and Richard (2002). Over the years, methodologies have been developed improving this process and the seismic inversion techniques have been adopted as an essential part in reservoir characterization workflows (Ferreira & Lupinacci, 2018; Penna & Lupinacci, 2021). However, it is necessary for the interpreter to insert relevant information, adding a geological meaning to the impedance volumes.

The level of geological details inserted depends on the methodology used. In this sense, the maximum amount of geological and physical information must be considered to optimize the cost versus benefit ratio of the seismic inversion process. Some methodologies, such as probabilistic inversions, can generate impedance volumes highly detailed (Avseth et al., 2005). However, the time required to prepare the data and the computational cost can be prohibitive.

In a way to integrate lithological data into a workflow that allows for improved reservoir characterization and, at the same time, that is robust enough to honor geological and geophysical properties, we present a study driven by rock physics modelling based on Elasto-Facies Association (EFA) scheme according to Kemper et al. (2016). Our analysis resulted in a new attribute derived through AVOImpedance technique (Simm et al., 2002), which combines the elastic responses and geological properties related mainly to diagenetic effects from analyzed rocks that have acted during the burial (Paiva, 2021). This 1D analysis can be used as a feasibility study to a 3D seismic inversion process, being an alternative workflow for laborious and time-consuming probabilistic facies classification techniques.

We applied this methodology in five wells drilled in the High Block of the Roncador Field - Campos Basin. Roncador Field is located in the northern portion of the Campos Basin, approximately 125 km from the coast of the state of Rio de Janeiro, with water column varying from 1500 to 1900 m (Pádua et al., 1998). According to

the Brazilian regulatory agency, Agência Nacional do Petróleo, Gás Natural e Biocombustíveis (ANP, 2021), this field is responsible for the sixth major daily oil production in Brazil, producing 132 Mboe/d and is the biggest siliciclastic producer field currently in activity (Fig. 1). The target of this study is the turbiditic reservoir RO 330. It is composed of trough confined gravel/sand-rich lobes of Maastrichtian age and it is the main producer system in this field (Bruhn et al., 2003). These turbidite sandstones are located in the Carapebus Formation, Tamoios Member (Fig. 2), having an average porosity and oil saturation up to 29% and 82% respectively. The oil gravity is between 17° and 31° API units (Rangel & Martins, 1998).

Elasto-Facies classification based on Depth Trend Analysis

Understanding the geological constraints is an important manner to reduce the range of expected variability in rock properties and hence reduce the uncertainties in seismic reservoir predictions. Along this study, we analyzed these constraints for an enhanced reservoir elastic response estimation. To apply rock physics modelling techniques properly, an accurate petrophysical evaluation must be conducted to define the total of parameters and the effective ones to estimate the volumetric fraction, porosity and water saturation, as shown in Figure 3. The advantage of this approach is that it allows defining petrophysical quantities in terms of mineralogy and/or lithology. Thus, total parameters are related to mineralogy, that is, their volumetric fractions correspond to mineral constituents, such as clay volume (V_{clay}) and the ratio of quartz volume to feldspar volume ($V_{\text{quartz}}/V_{\text{feldspar}}$). Meanwhile, effective parameters are related to lithological members, defining the lithological volumes, such as V_{shale} and V_{sand} .

To start the geological investigation through the elastic responses, we removed hydrocarbon effects from reservoir rocks, using Gassmann fluid substitution (Gassmann, 1951) and simulated a new scenario with 100% brine saturation for P-wave velocity (V_p), S-wave velocity (V_s) and Density (RhoB) logs. Fluid properties were calculated using

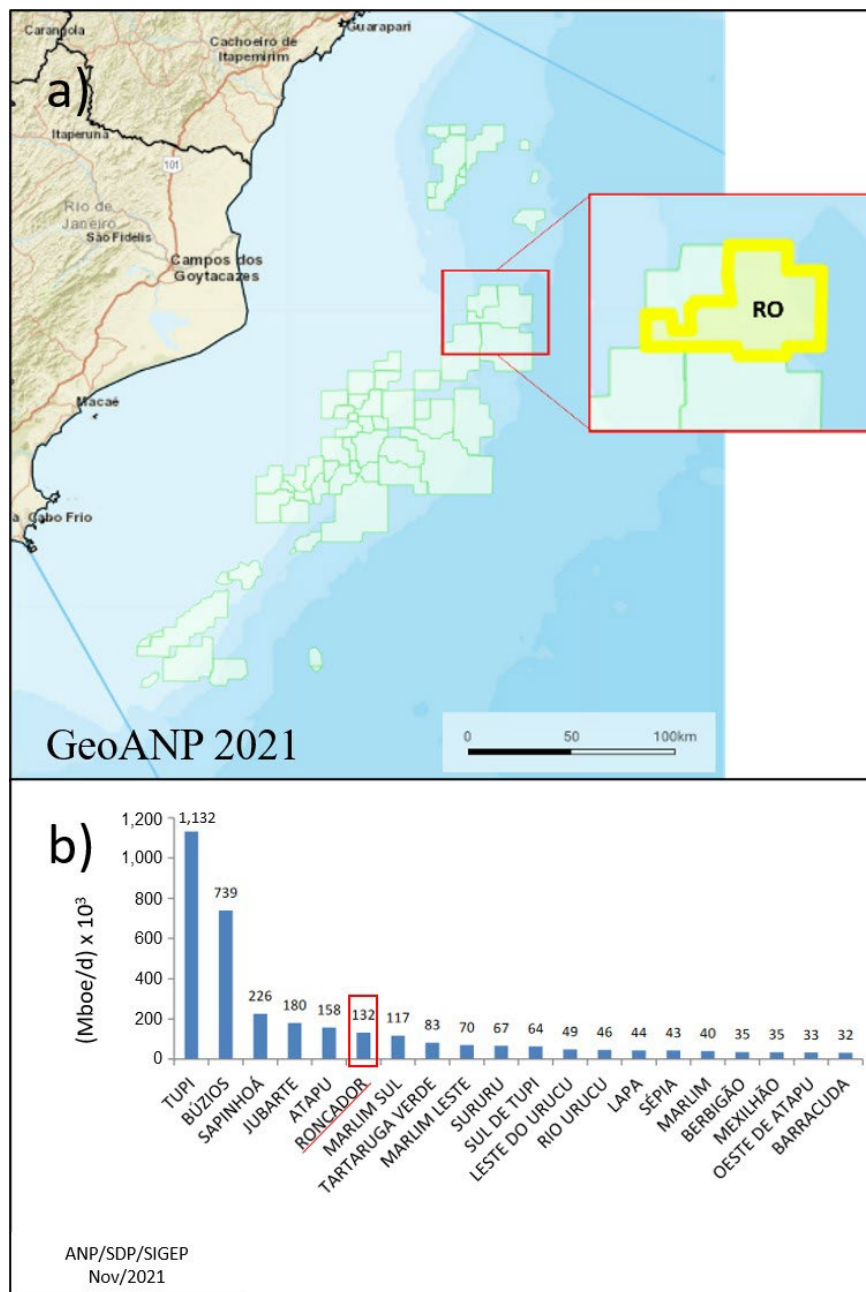


Figure 1 - 1a) Map of Campos Basin highlighting the location of the Roncador Field. Figure 1b). Daily production histogram where Roncador Field is the sixth biggest producer and the main siliciclastic field producer currently in activity (Adapted from Monthly Production Report – ANP, 2021).

FLAG fluid calculator (Batzle & Wang, 1992), where the parametrization was conducted according to the well documentation: effective pressure = 31MPa; temperature = 70°C; salinity = 87.000 ppm.

Analyzing the depth trends (TVDml – True Vertical Depth bellow Mudline) for V_p brine, we verified the existence of two main trends for reservoir and non-reservoir rocks. These trends evidence geological properties related to effects of diagenesis that act on compressional velocity (V_p) (Figs. 4a and 4b). We established cuts of $V_{clay} \leq 15\%$ for the

reservoir rock (sandstones) dataset and of $V_{clay} > 85\%$ for non-reservoir rocks (shales). In this way, we proposed an Elasto-Facies classification based on V_p variation with depth. Since velocity-depth trends are mainly controlled by diagenetic effects (Simm & Bacon, 2014), we applied this methodology to capture the elastic responses related to geological properties for reservoir and non-reservoir rocks, as shown in Figures 4c and 4d. For reservoir rocks, we associated the sandstone clusters in five Elasto-Facies with Sand B and Sand C laid down in the

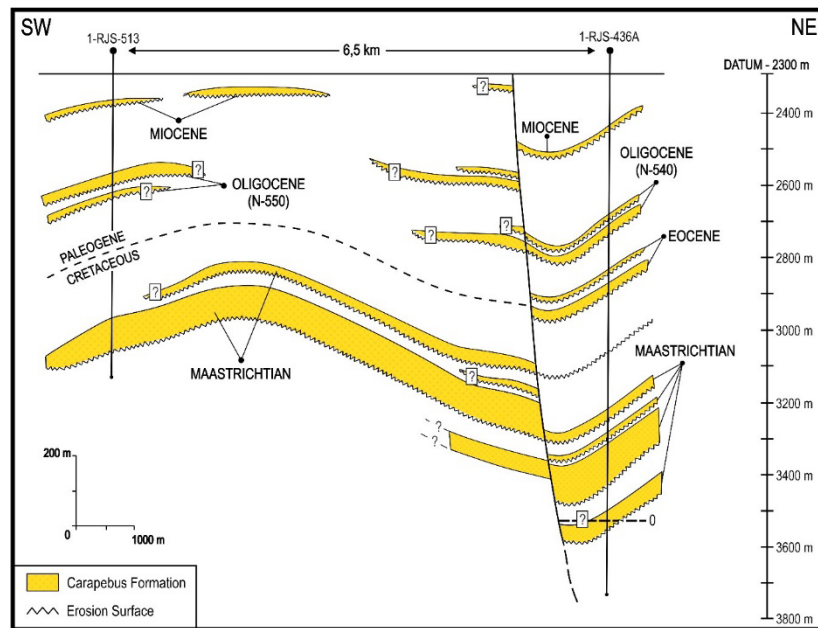


Figure 2 - Geological scheme with the main geochronological features of the Roncador Field (Adapted from Rangel & Martins, 1998).

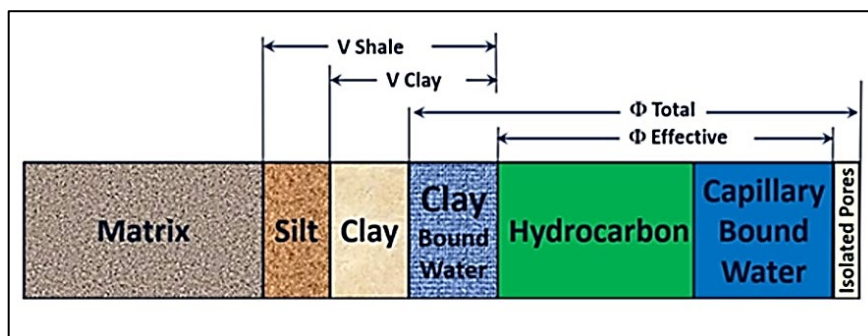


Figure 3 - Schematic definition of petrophysical properties suitable for rock physics modelling and their relationship with rock and fluid elements (Adapted from Simm & Bacon, 2014).

upper and lower main trends, respectively. These clusters came mostly from the interval RO 330. Sand A is a small sandstone clustering from interval RO 200, slightly deviated from the upper main trend. Sand D and Sand E are the clusters with high V_p values from the shallowest and deepest part, respectively, slightly far from their correspondent main trend, also with major contributions from interval RO 330 and a few from RO 400. Similarly, we associated the non-reservoir rocks in three Elasto-Facies defined as Overburden, Underburden and Intra-reservoir, where Overburden and Underburden are the shales correspondent from the upper and lower trends, respectively. Intra-reservoir facies are the identified

thin shale laminations interbedded into RO 330.

This analysis resulted in a well log curve named Elasto-Facies Association (EFA), capable to represent the lithofacies classified in terms of their elastic responses regarding its geological properties, although these properties are strongly influenced by local geological trends that are related to depositional environment or burial history (Avseth, 2000). Thus, we verified that lithology logs from mudlogging data together with petrophysical curves have a direct correlation with EFA logs. This proves that we have been successful to integrate lithological data and petrophysical properties into our geophysical analysis (Fig. 5). However, in non-reservoir lithologies, this analysis was only able to

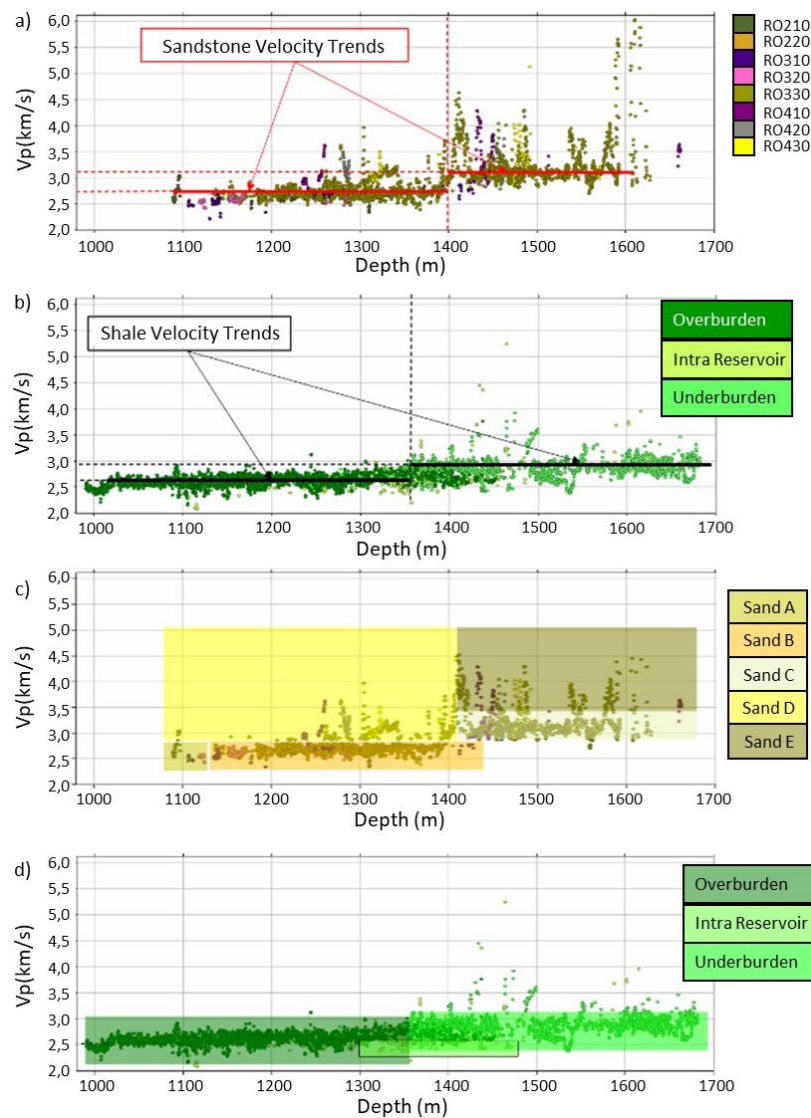


Figure 4 - The depth trend analysis for velocities clearly showed two main trends for sandstones (a) and shales (b). In (c) and (d) we have the EFAs defined based on velocity behavior for reservoir and non-reservoir rocks respectively.

capture the main shaly end member, due to the low elastic contrast verified with the marls. For this reason, marls were grouped as a generical non-reservoir elasto-facies.

Diagenetic Effects Modelling through Rock Physics Models

To understand how geological properties influence the elastic responses, Paiva (2021) applied cementation rock physics models¹ (Avseth et al., 2005) on the sandstone influence, according to the proposed EFA. We used the total of petrophysical parameters following Vernik (2016). Figure 6

displays the analysis of all EFAs of reservoir intervals from Maastrichtian turbidites, over a cementation perspective from a Vp versus total porosity (PHIT) plot. Through this modelling, we verified that there is no presence of unconsolidated sands or highly cemented sands. In fact, it is an analytical confirmation that Maastrichtian turbidite reservoirs of the Roncador Field are composed essentially of poorly consolidated sands (Bruhn et al., 2003). These observations indicate that cementation does not play a major role in explaining how geological properties affect elastic responses.

¹ Constant Cement Model and Contact Cement Model

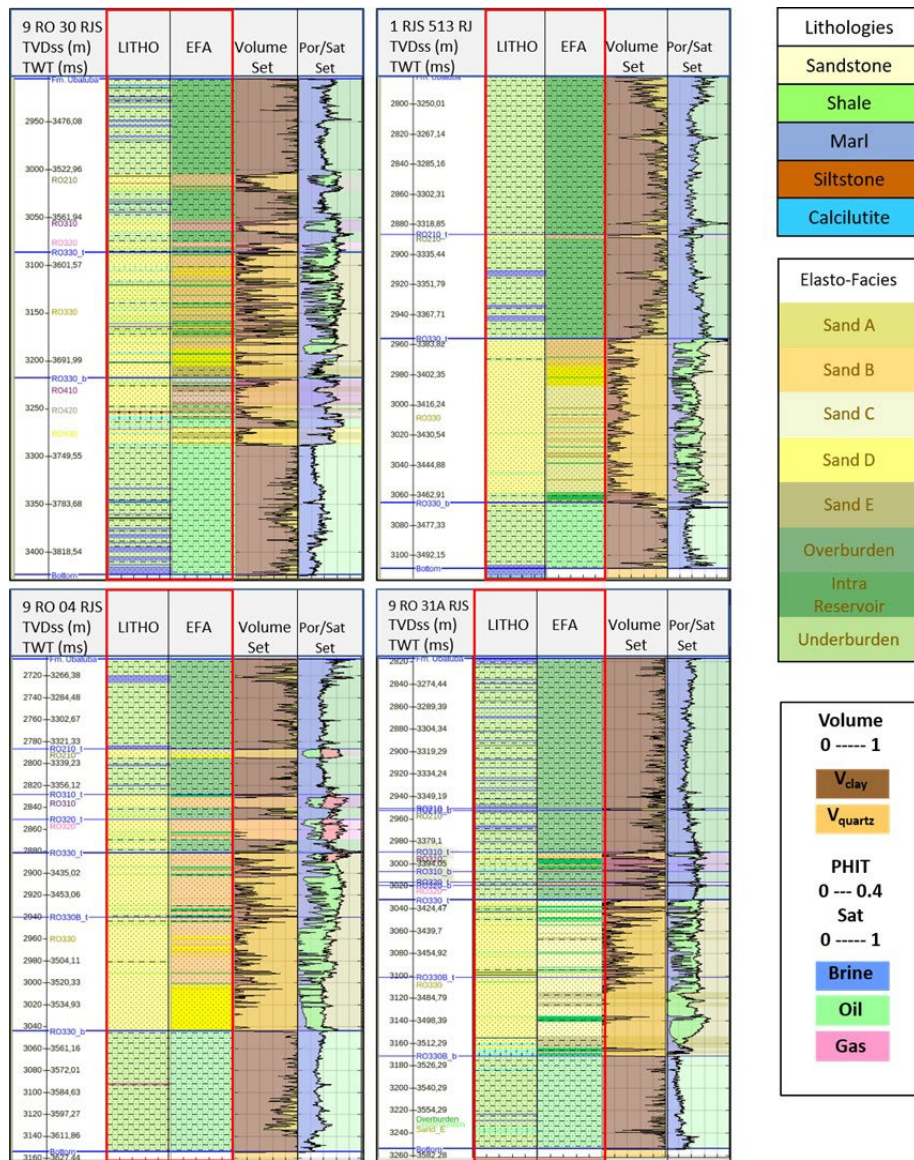


Figure 5 - Display of Lithological data, petrophysical property set² and EFA curves for some Wells analyzed in this project showing a strong correlation between them.

The increase in velocity can be explained mainly by grain sorting, in which the smaller grains fill the pore space among the larger ones, consequently decreasing the porosity. In this same study, through Friable Model for Shales, Paiva (2021) demonstrates that smectite is the dominant clay mineral type in the shales of the Underburden interval, due to mechanical compaction, which is also responsible for the increase in velocity in the lower trend for non-reservoir rocks.

1D AVO Forward Modelling and Seismic Amplitude Interpretation

Once understanding the effects of geological properties on elastic responses, the next step aims to verify how this impacts the seismic amplitudes. We applied this analysis to the interfaces defined from the intervals:

- Interface 1 – Overburden (Upper Layer)/RO 330A (Lower Layer).
- Interface 2 – RO 330A (Upper Layer)/RO 330B (Lower Layer).

² Property set is a combination of information creating a unique normalized curve for the analyzed property. Here, Volume Set was created through V_{clay} log complemented by the V_{quartz} properties to fill the difference. Por/Sat Set plots Sw information in the Porosity log (PHIT) complemented by the pore fluid fill content information.

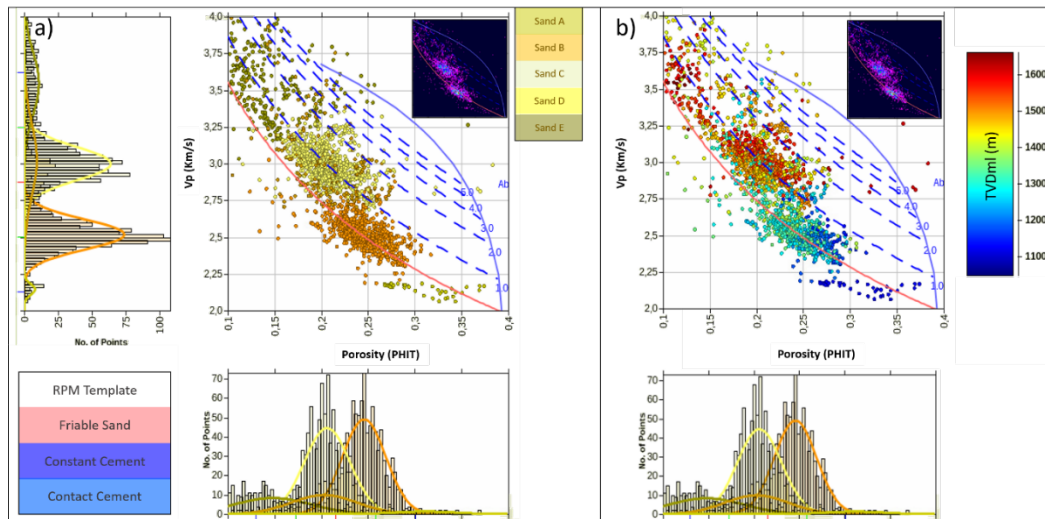


Figure 6 - Velocity – porosity analysis with cementation models superimposed, colored by EFAs (a) and depth (b). The histograms display the distribution of each elasto-facies for Vp and PHIT. The point density visualization is visible in the upper right corner of each plot.

- Interface 3 – RO 330B (Upper Layer)/Underburden (Lower Layer).

We analyzed the most significant interfaces for seismic interpretation and reservoir characterization. In this case, we defined the top and base interfaces of the main producer (RO 330) and a secondary interface that splits this interval into RO 330A and RO 330B, as illustrated in Figure 7 for Well 9 RO31A RJS. This process involved plot reflection coefficients calculated using Zoeppritz equation (Aki & Richards, 2002) against incidence angle to model 1D AVO responses for in situ and 100% brine saturated cases. No wavelet was used in this step.

To accurately model seismic amplitude along the interfaces, we used a deterministic wavelet estimation extracted from seismic data using White & Simm (2003) methodology. Considering a good well-tie, this technique produces a wavelet that honors the seismic amplitude scales, frequency content and phase information. The estimated wavelet presented a phase rotation of -40° and a time delay of -4ms , where we assigned this phase effect mainly to the huge oil-sand saturated interval. Then, we created synthetic angle gathers (through the convolution between the estimated wavelet and the reflection coefficient) for both saturation scenarios. Finally, we compared the real amplitudes with the synthetical one along the interfaces defined above. This analysis is illustrated in Figure 8,

where we also inserted EFAs, mineral volume set ($V_{\text{clay}}/V_{\text{quartz}}$) and saturation set (PHIE & Sw/complements) curves, adding geological and petrophysical information to aid the geophysical interpretation.

Then, we applied the AVO classification proposed by Rutherford & Williams (1989), Ross & Kinman (1995) and Castagna & Swan (1997). AVO interpretation must be conducted with care once there is nothing about its significance that allows generalizing it. The geological context is clearly very important for this type of analysis. To understand the significance of different AVO responses, we created models for different scenarios and compare the results with seismic observation, as mentioned previously. The AVO class response is not the most important, but the relative change in AVO responses. Thus, we can interpret the seismic amplitude behavior along a reflector or interface, which is the most valuable information extracted from this analysis.

The AVO response for interfaces 1 and 2 is class I, which is characterized by a positive reflection coefficient that decreases with the increasing incidence angle (negative gradient). This effect could be addressed to the hydrocarbon presence in less fluid sensitive sandstones, causing an attenuation of seismic amplitudes (Simm & Bacon, 2014), as shown in the top reservoir. It may raise issues related to the similarity of AVO curves, where the models seem

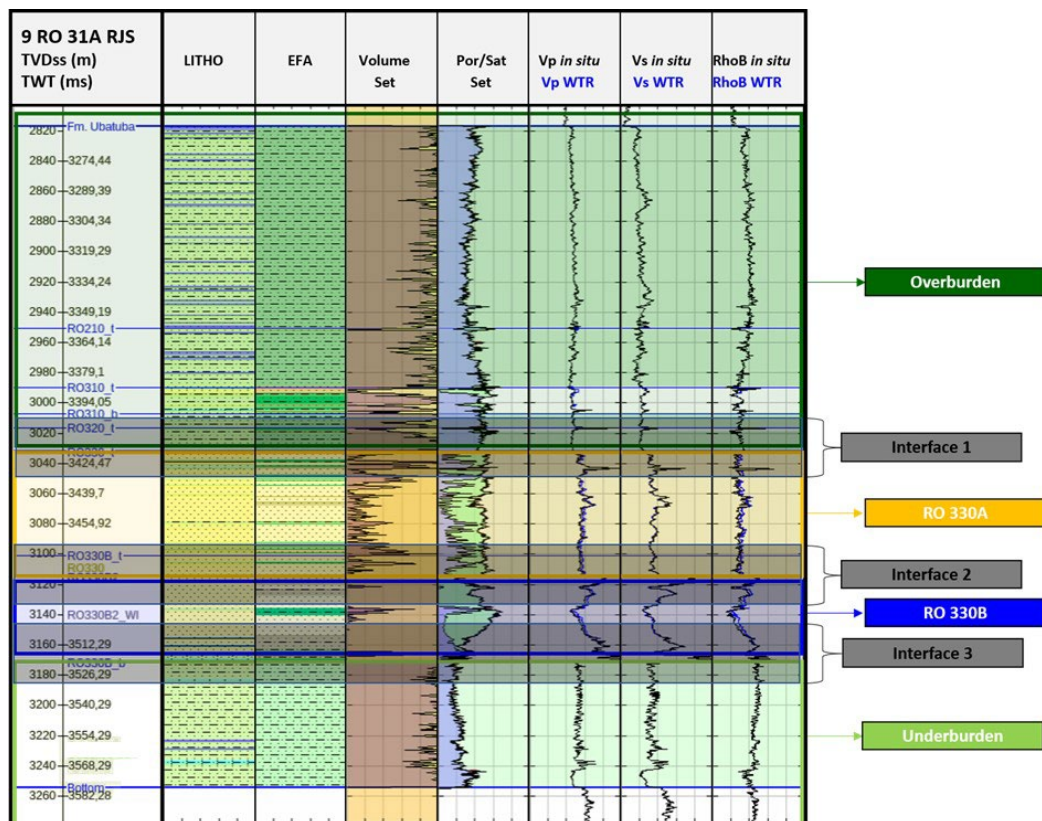


Figure 7 - Target zones with main interfaces of interest defined in the top of reservoir RO 330 (Interface 1), the intermediary interface that split RO 330 into RO 330A and RO 330B (Interface 2) and Interface 3 at the base of the reservoir for well 9 RO 31A RJS.

to be shifted in comparison between them for both saturation scenarios in interface 1. This effect could in principle be explained by hydrocarbon parameters, as low API and high GOR. Interface 3 presents a class IV AVO response for in-situ and brine saturation, that is, the reflection coefficients are negative and become less negative with the increasing incidence angle. However, the gradient variation is less perceptible for the brine scenario, being almost constant, meaning that brine substitution does not cause noticeable variations along the angle range. Class IV AVO response is often associated to reservoir sandstone base (Simm & Bacon, 2014). The mineralogy and fluid changes are the main responsible for the decrease in acoustic and shear impedances in the lower layer. The effect of these negative elastic parameter variations in AVO plot results in a negative intercept and a positive gradient.

The reflection coefficients at interfaces 1 and 3 show little variation along the offset in near and middle angles for in-situ and brine scenarios. This means that the near and middle impedances

(Acoustic Impedance - AI and Shear Impedance - SI) are not completely able to differentiate whether the reservoir is in in-situ conditions or 100% saturated with brine. However, in the reflection coefficients for the far angles, there is an indicative of enough contrast to differentiate these scenarios. Therefore, far impedances such as Elastic Impedances (2 terms) and Lamé's parameters (Mavko et al., 2009) provide additional information to aid this analysis. Our analyzes are limited to incidence angles up to 30°. For larger angles, the effect of divergence in the AVO curves is observed, which is characteristic of the modeling using the Zoeppritz equation (Aki & Richards, 2002).

Interface 2 presents little variation of the reflection coefficient for both scenarios along the angle ranges. This demonstrates that there is no sensitivity to fluid change at this interface. However, the reflection coefficients (absolute values) are higher than the values observed for interfaces 1 and 3; thus, we should expect relatively high impedance values and a perceptible seismic reflection along this interface.

The fullstack seismic data has an angle range of 5° to 32°, so we chose the angle of 17° (medium angle stacking) as the representative angle. Then, we plotted the seismic data with the synthetic trace stacked at 17° along the well path to support this analysis. Synthetic data show a good correspondence with real data in terms of polarity and amplitude. However, there are some divergences, more noticeable for interface 3 in the middle-far angle range (above 20°). This can be explained by wavelet characteristics such as phase rotation and mainly due to time delays, as mentioned earlier. We have a good fit if we disregard the time delay, interpreting the reservoir base in the seismic data 4ms lower than in the well data.

1D Impedance Contrast Analysis

In this session, we took a different approach from the previous one to analyze the seismic amplitude interpretation regarding elastic parameter modelling. Here, the impedances are analyzed in terms of contrasts along the same interfaces and saturation scenarios defined earlier. Impedance contrasts are defined as a ratio between the impedance measured in the upper and lower layers along a given interface:

$$\frac{(\text{Imp}_{\text{lower}} - \text{Imp}_{\text{upper}})}{(\text{Imp}_{\text{lower}} + \text{Imp}_{\text{upper}})}, \quad (1)$$

where $\text{Imp}_{\text{upper}}$ and $\text{Imp}_{\text{lower}}$ are respectively the impedances of the upper and lower layers. The reason for this analysis is to know which of the impedances can provide useful information for the reservoir characterization. We analyzed the behavior of elastic parameters such as V_p , V_s and density in terms of near, middle and, mainly, far impedances, since in the study area the farther angles are more sensitive to fluid substitution.

We set the threshold angle to 30° for the elastic attribute calculations (threshold where the divergence effect becomes more visible according to the 1D AVO curves in Fig. 8). Thus, the impedance contrast analysis with respect to the parameters discussed is illustrated in Fig. 9 for the following quantities: AI (Acoustic Impedance), SI (Shear Impedance), EI2_30° (Elastic Impedance –

2Terms), SEI2_30° (Shear Elastic Impedance), M (P-wave Modulus), μ (Shear Modulus), K (Bulk Modulus), σ (Poisson's Ratio), λ (Lamé's first parameter), $\lambda\rho$ (LambdaRho), $\mu\rho$ (MuRho) and λ/μ (LambdaOverRho). Although we have calculated all these quantities (impedances and elastic modulus), our analysis is restricted to impedance contrast responses, since they are commonly used in reservoir characterization studies.

As expected, interfaces 1 and 3 present changes in saturation scenarios. Since the modeling is related to the contrasts defined by Eq. 1, the values obtained are small. Even so, a significant variation for AI, EI2_30°, Poisson ration, LambdaRho and Lambda/Mu is noticed. An interesting observation concerns the far impedances, which for interface 1 presented a huge variation (EI2_30° = 157% and LambdaRho = 321%). The five elastic impedances have a high sensitivity to fluid, demonstrating the importance of carrying out this study for the Roncador Field reservoir. At interface 2, no variation in impedance contrasts is observed in relation to the fluid type. However, the impedance contrasts are higher (absolute values) compared to the contrasts at interfaces 1 and 3 for AI, EI2_30° and LambdaRho. This indicates that impedances can be useful for lithological discrimination in this reservoir interval.

Petro-Elastic Property Analysis based on EFA Classification

The objective now is to understand how petrophysical properties are linked to EFA and, consequently, to elastic responses. For this, we integrated all the analyzes carried out in the previous sections. Here, we used geological knowledge to classify EFAs in relation to reservoir properties. This analysis was performed through the crossplots of impedance responses *versus* petrophysical properties from well logs for reservoir and non-reservoir rocks (Fig. 10). The EFAs related to reservoir rock clusterings were analyzed in terms of PHIT and $V_{\text{clay}} \leq 0.35$ (Figs. 10a and 10b respectively). Non-reservoir rock clusterings were plotted only for $V_{\text{clay}} \geq 0.7$ (Fig. 10c).

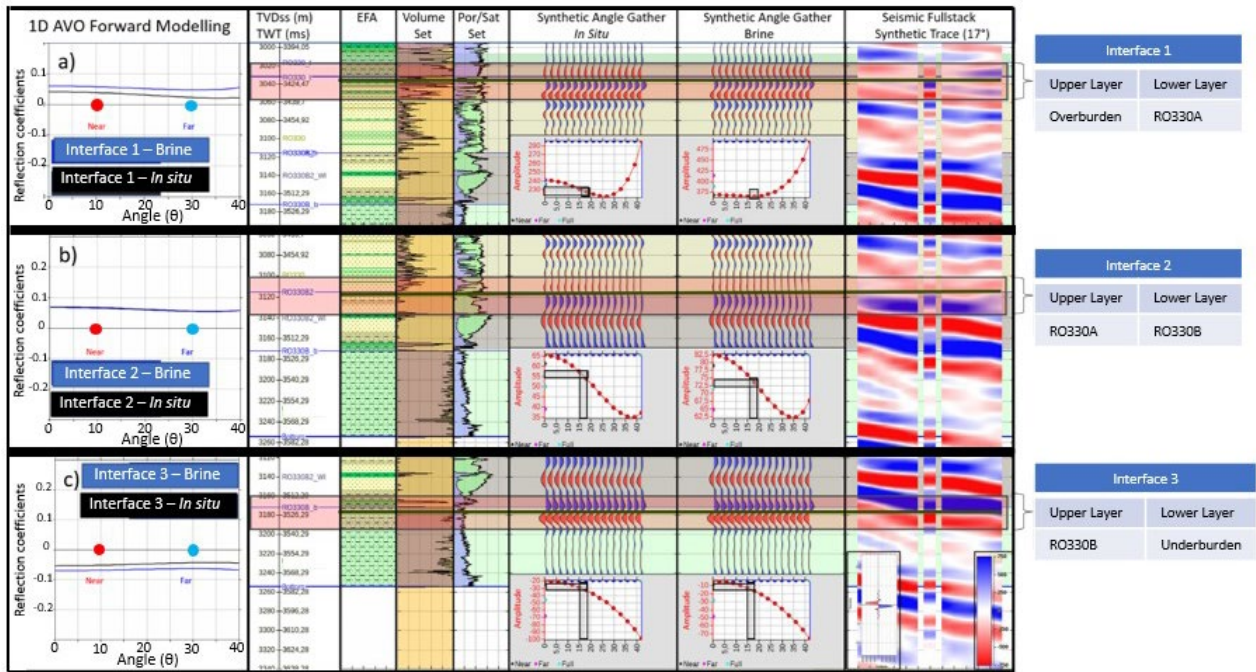


Figure 8 - 1D AVO & Synthetic forward modelling analysis for amplitude interpretation based on the reflection coefficients and synthetic modelling over the interested interfaces. EFAs, Volume (V_{clay} & V_{quartz}) and Por/Sat (PHIT & $Sw/complements$) set curves are displayed to support the interpretation along the well column.



Figure 9 - Elastic contrast analysis showing impedance and elastic modulus variation for fluid scenarios at each interface. The tables at the right of each scenarios display the values for considered impedances and the variation regarding in situ to brine cases.

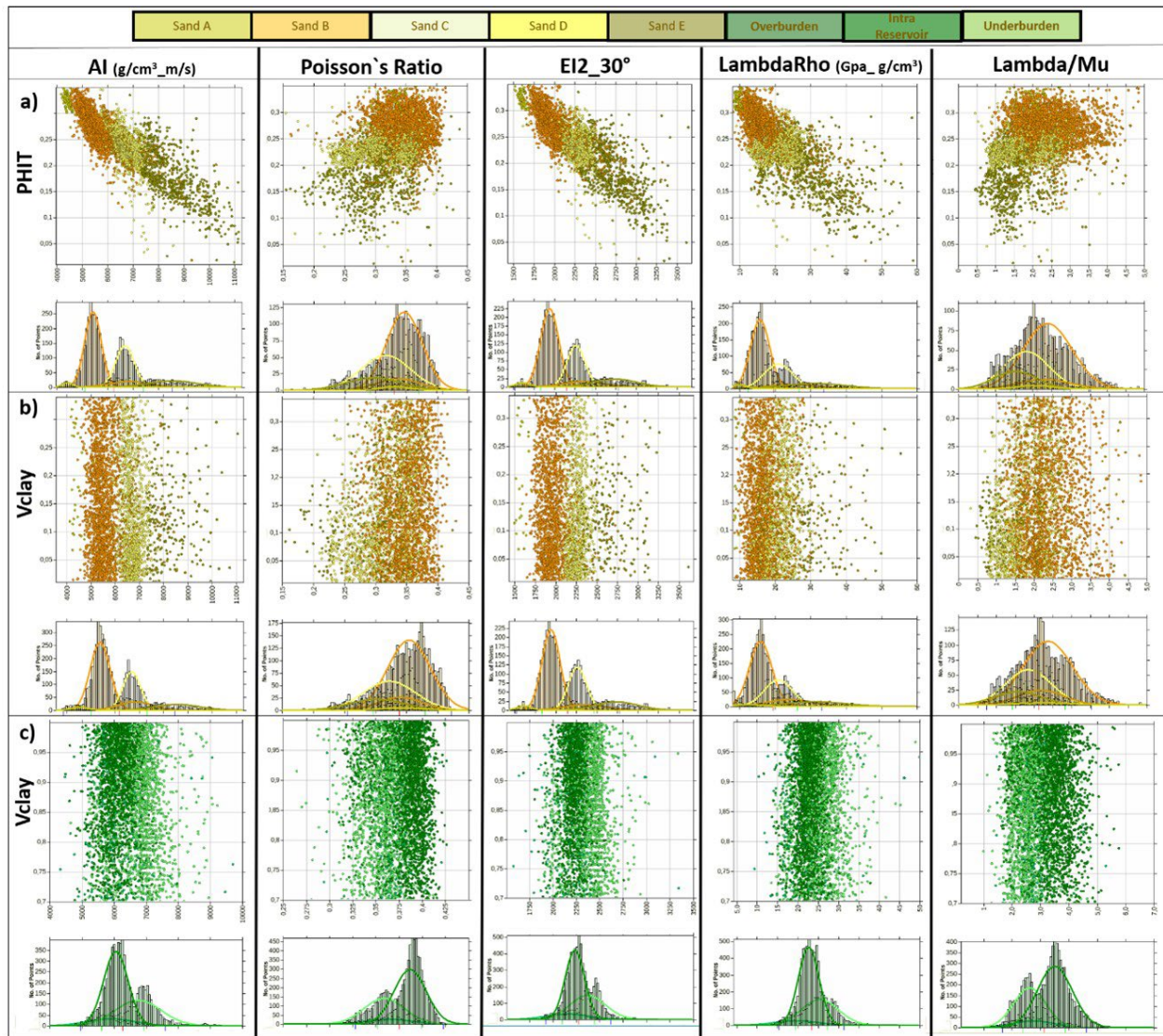


Figure 10 - Elastic attribute responses through petrophysical property analysis parametrized by EFAs. Reservoir responses can be verified in terms of PHIT (a) and V_{clay} (b). Non reservoir response is only available for V_{clay} (c).

We can verify for the reservoir rocks that the Sand B and Sand C elasto-facies are easily discriminated in the elastic spaces AI and EI2_30°. It is also possible to discriminate the Sand A and Sand E facies using these same elastic spaces. However, these elastic spaces did not provide a discrimination for Sand C and Sand D. The analysis of the histogram shows that Sand D is practically in superposition with Sand C, not being possible to distinguish them. For the other impedances (Poisson's Ratio, LambdaRho and Lambda/Mu), we did not observe any discrimination due to the high degree of overlap between the EFAs. For non-reservoir rocks, we do not observe any discrimination, regardless of the elastic half-space considered. The only possible

analysis was to verify which of the elastic attributes has the minimum overlap. We chose the same elastic space AI and EI2_30° based on the histograms.

AVOImpedance (AVOI) Technique application through Weighted Stack Crossplot Analysis

After analyzing that AI and EI2_30° have a direct correlation between EFAs, geological properties and petrophysical quantities, it became clear that the analyzed intervals, mainly RO 330, have a seismic amplitude response highly dependent on AVO phenomena. For this reason, near and far impedances proved to be the best elastic

quantities for characterization of this interval in terms of impedances. This way, we proposed the usage of AVOImpedance technique (Simm et al., 2002), which is described as a data adaptative method based on the combination of near and far impedances weighted by a third³ quantity, thus generating a new attribute from this procedure. Since the formulation of elastic impedance (Connolly, 1999), several works have demonstrated the benefits of extracting combinations of elastic parameters with the exploitation of AVO phenomena that provide greater discrimination of fluids and lithologies (Goodway 2001; Mukerji et al., 2001; Whitcombe et al 2002; Veeken & da Silva, 2004).

Analyzing the AI versus EI2_30 elastic half space graph weighted by volume fraction curve V_{clay} , we performed the rotation of the symmetry axis to create a projection for discrimination of EFAs, as shown in Figure 12, where the reservoir EFAs are displayed. Through this analysis we extracted a math relationship (linear equation) that is able to correlate the geological, physical and petrophysical properties for reservoir rocks given by:

$$Pjtn_{\text{RSV}} = -1.8823 * AI - EI2(30^\circ) + 13794.3. \quad (2)$$

After defining the relationship for reservoir rocks, we extended this analysis to non-reservoir rocks. However, it was not possible to establish a correlation for these rocks. Then, we observed that, at least, it is possible to discriminate the main reservoir interval RO 330 from non-reservoir intervals (Overburden and Underburden) as shown in Figure 11, through the following mathematical relationships:

$$Pjtn_{\text{Over}} = 0.2526 * AI - EI2(30^\circ) + 665.46, \quad (3)$$

$$Pjtn_{\text{Under}} = 0.2455 * AI - EI2(30^\circ) + 697.47. \quad (4)$$

Figure 13 presents the distribution of the attribute projection in terms of EFAs weighted by V_{clay} . The observed overlap for Sand C and Sand D sand facies remains. However, some overlaps that emerged when we included all EFAs need attention and they were treated as follow: The case

of Sand B and Intra-Reservoir facies was considered as unsolved, since the latter represents laminations of intercalated shales along the RO 330 interval, not being possible to distinguish it in terms of elastic parameters of Sand B. Also, we expected Intra-Reservoir facies to be undetectable at seismic scale due to the low thickness. For this reason, the Intra-Reservoir facies was neglected in the final attribute.

It is important to mention that we are not considering the intervals RO 200 (RO 210, RO 220, RO 230), RO 400 (RO 410, RO 420, RO 430) and the subdivision of RO 300 (RO 310, RO 320), since they are essentially small sandstone laminations. This means that the calibrations were performed with the RO 330 interval, and we extended this to the other intervals. Thus, these other ones must be interpreted with care. The overlap treatment and posterior classification of the Overburden and Underburden elasto-facies were more complicated because the elastic parameter responses of these facies are very similar. The geological and geophysical characterization of these facies is extremely important for the study area. As we consider the Overburden and Underburden as the non-producing intervals above and below the RO 330, respectively, their stratigraphic interpretation is mandatory in the wells and important in the seismic data (if a seismic inversion study is the main objective) for the correct application of this methodology. The strategy adopted was to consider the range values of both EFAs, allowing them to assume the values centered on their respective averages, but varying around the standard deviation. This prevented them from assuming similar values in their own range values. Thus, we were able to restrict their range limits and both EFAs assumed different values, being distinguishable from each other.

Each elasto-facies assumed specific range values, as illustrated in Figure 14, except for the unsolved cases for Intra-Reservoir & Sand B and Sand C & Sand D. Finally, we considered that the

³ This technique supports several types of geological, petrophysical and geophysical data.

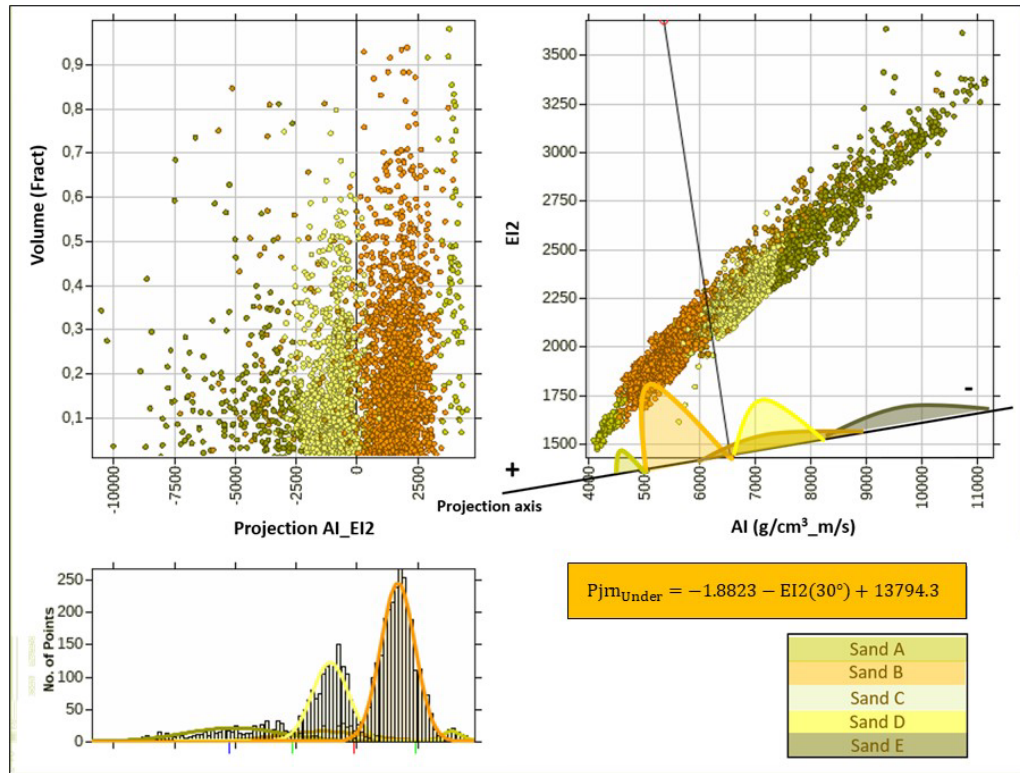


Figure 11 - AVOI projection attribute between AI and EI2_30° weighted by V_{clay} curve for all reservoir EFAs.

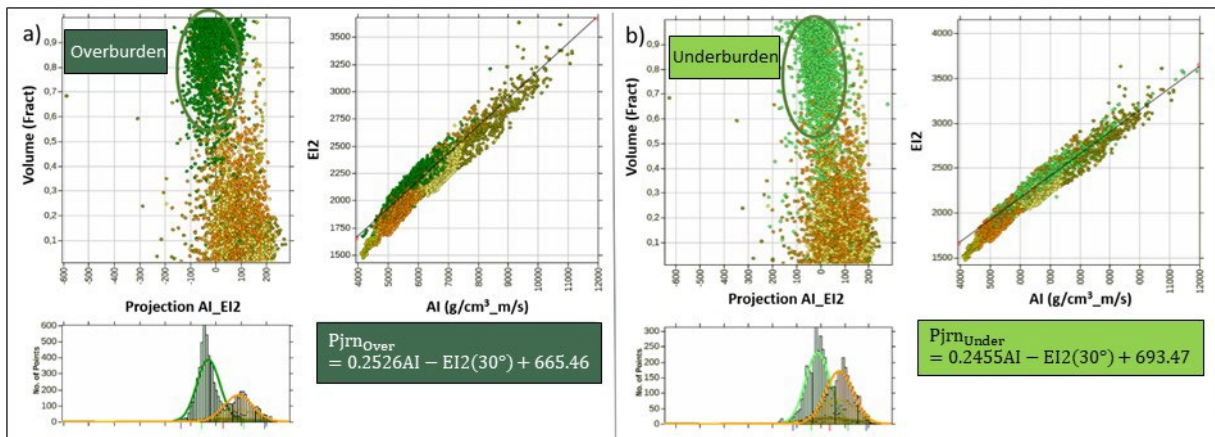


Figure 12 - AVOI projection attribute between AI and EI2_30° weighted through V_{clay} displaying the analysis for non-reservoirs Overburden (a) and Underburden (b) jointly with all reservoir EFAs.

Overburden & Underburden case was satisfactorily resolved, since the restricted range kept the values without overlap between both elasto-facies, allowing them to be discriminated.

Lithological Discrimination Attribute generated through the integration of geological, physical and petrophysical properties

We generated the Lithological Discrimination Attribute (LDA) as a result of the integration of lithological data (Lithology log), diagenetic effects, petrophysical properties and elastic parameters,

performing a new attribute, which has a strong correlation and discrimination of EFAs from reservoir properties. Figure 15 illustrates this analysis by comparing the properties and the modeled LDA, showing very consistent results. Inspecting the LDA curve, we observed a correlation between the EFA curves and the lithology logs. Seismic data and petrophysical properties are displayed here to add more robustness to our analyses.

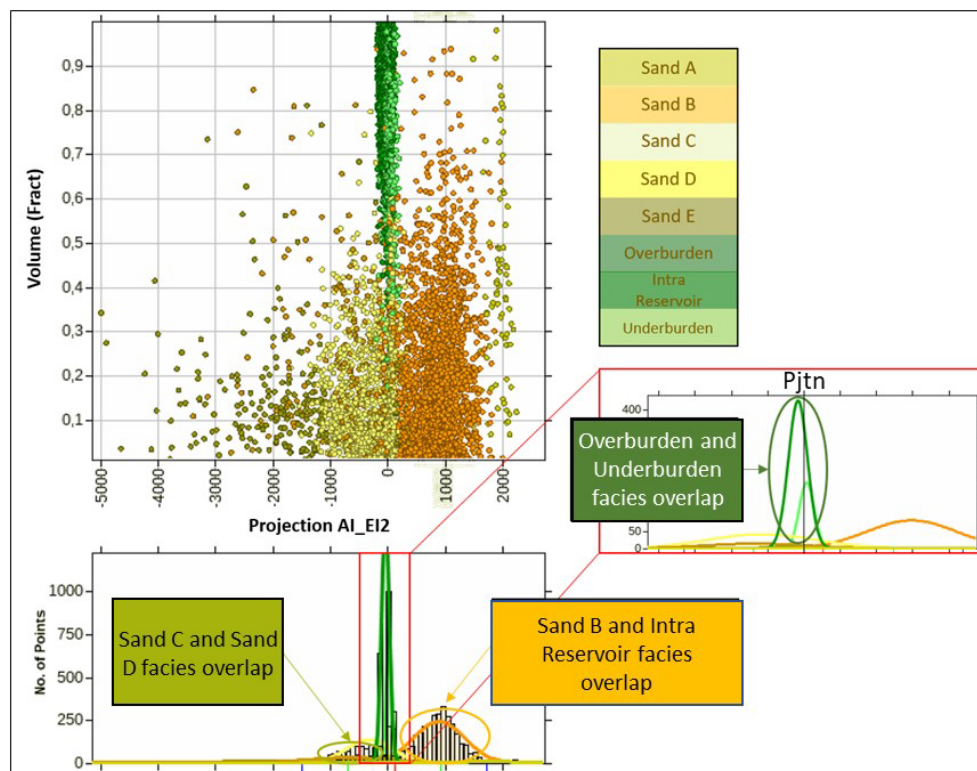


Figure 13 - AVOI projection attribute between AI and EI2_{30°} weighted through Vclay displaying the analysis for non-reservoirs Overburden (a) and Underburden (b) jointly with all reservoir EFAs.

We applied the methodology in other wells that do not have lithological data (lithology log). We performed this as a test of the methodology's predictive capacity in a scenario of lack of this information. This analysis is shown in Figure 16, where once again we can see a strong correlation of the EFA curves and petrophysical properties with the LDA logs. This indicates that the methodology has robustness to model and predict the LDA curves, integrating the domains of geology, petrophysics and geophysics.

CONCLUSIONS

We presented an extensive and methodical workflow using the well data to aid in seismic amplitude interpretation, which is driven by rock physics modeling for the characterization of the Roncador Field reservoir in terms of elastic responses and petrophysical properties. Through rock physics modeling, we analytically demonstrated that Maastrichtian turbidites of the Roncador Field are composed essentially of poorly consolidated sands, where grain sorting is the main porosity reduction mechanism instead of cementation. Non-

reservoir rocks are over mechanical compaction effects, which act more notably in the Underburden interval. From this investigation, we understood the main diagenetic effects acting on and controlling the elastic responses of the studied intervals. This way, the elastic responses were modelled in terms of reflection coefficients, synthetic amplitudes and impedance contrasts, where we verified that all important answers from these models are highly responsive to the AVO phenomena and, at the same time, can be directly correlated to petrophysical properties. In this way, it became possible to successfully integrate the domains of geology, petrophysics and geophysics to be used as a feasibility study for seismic inversion supporting the reservoir characterization process. To minimize the effects of overlap among EFAs, we recommend that this study should be supported by a geological interpretation for a more accurate calculation of the LDA. Finally, we propose to extend this workflow to a 3D analysis, as it has been shown to be robust for EFA discrimination, being less costly than workflows based on probabilistic seismic inversion methodologies.

ACKNOWLEDGMENTS

The authors are grateful to the Brazilian National Agency of Petroleum, Natural Gas and Biofuels (ANP) for the provision of seismic and well data used in this research as well as to Ikon Science Limited and Schlumberger for providing academic environment software access for the development of this study. The authors also sincerely thank Rafaella Antunes for her support in formatting some figures. Likewise, the authors would like to thank the Instituto Nacional de Ciência e Tecnologia de Geofísica do Petróleo (INCT-GP/CNPq), Fundação Carlos Chagas Filho de Amparo à Pesquisa do Estado do Rio de Janeiro (FAPERJ), and the Coordenação de Aperfeiçoamento de Pessoal de Nível Superior (CAPES) for supporting this research. We also thank two anonymous reviewers for the time and dedication to improve this manuscript.

REFERENCES

- AKI K & RICHARDS PG. 2002. Quantitative Seismology. University Science Books, 2nd ed., 700 pp.
- ANP. 2021. Boletim da Produção de Petróleo e Gás Natural. [Monthly Production Report]. Superintendência de Desenvolvimento e Produção - SDP. Agência Nacional do Petróleo, Gás Natural e Biocombustíveis. Rio de Janeiro, Brazil. March 2021. n. 127. 40 pp.
- AVSETH P. 2000. Combining rock physics and sedimentology for seismic reservoir characterization of North Sea turbidite systems. PhD thesis, Stanford University. 181 pp.
- AVSETH P, MUKERJI T & MAVKO G. 2005. Quantitative Seismic Interpretation: Applying Rock Physics Tools to Reduce Interpretation Risk. Cambridge University Press, 359 pp.
- BATZLE ML & WANG Z. 1992. Seismic properties of fluids. *Geophysics*, 57(11): 1396-1408. DOI: 10.1190/1.1443207.
- BRUHN CHL, GOMES JAT, LUCCHESI JR CD & JOHANN PRS. 2003. Campos Basin: Reservoir Characterization and Management – Historical Overview and Future Challenges. Offshore Technology Conference, OTC-15220-MS, Houston, Texas, USA, 5-8 May.
- CASTAGNA JP & SWAN HW. 1997. Principles of AVO crossplotting. *The Leading Edge*, 16: 948–956.
- CONNOLLY P. 1999. Elastic impedence. *The Leading Edge*, 18(4): 438–452. DOI: 10.1190/1.1438307.
- FERREIRA DJA & LUPINACCI WM. 2018. An approach for threedimensional quantitative carbonate reservoir characterization in the Pampo field, Campos Basin, offshore Brazil. *AAPG Bulletin*, 102(11): 2267–2282. DOI: 10.1306/04121817352.
- GASSMANN F. 1951. On Elasticity of Porous Media. Zürich. In: PELISSIER MA, HOEBER HENNING, VAN DE COEVERING N, JONES IF. 2007. *Classics of Elastic Wave Theory*. Chapter 3p. Geophysics Reprints Series: p. 389–408.
- GOODWAY B. 2001. AVO and Lamé constants for rock parameterization and fluid detection, *CSEG Recorder*, 26(6): 39–60.
- KEMPER M, ABEL M, De ROS LF & HANSFORD J. 2016. Integration of Lithological Data for Advanced Seismic Inversion. In: Third EAGE/SBGf Workshop 2016. Conference Proceedings. Rio de Janeiro, Brazil. DOI: 10.3997/2214-4609.201600059.
- MAVKO G, MUKERJI T & DVORKIN J. 2009. Rock physics handbook: Tools for seismic analysis in porous media. Cambridge University Press, 2nd ed., chapter 3, p. 81–168. DOI: 10.1017/CBO9780511626753.
- MUKERJI, T., JORSTAD, A., AVSETH, P., MAVKO, G. AND GRANLI, J. R. 2001. Mapping lithofacies and pore-fluid probabilities in a North Sea reservoir: seismic inversions and statistical rock physics. *Geophysics*, 66: 988–1001.
- PÁDUA KGO, STANK CV, SOARES CM & MOREIRA JV. 1998. Roncador Field, Strategy of Exploitation. In: Offshore Technology Conference, Houston, Texas, OTC-8875-MS, Houston, Texas, USA. DOI: 10.4043/8875-MS.
- PAIVA MFB. 2021. Modelagem de Física de Rochas e Análise dos Coeficientes de Reflexão e dos Atributos Elásticos dos Reservatórios Turbidíticos Maastrichtiano do Campo de Roncador, Bacia de Campos. Master Dissertation.

- Programa de Pós-Graduação em Dinâmica dos Oceanos e da Terra, Universidade Federal Fluminense, RJ, Brazil. 192 pp.
- PENNA R & LUPINACCI WM. 2021. 3D modelling of flow units and petrophysical properties in Brazilian presalt carbonate. *Marine and Petroleum Geology*, 124: 104829. DOI: 10.1016/j.marpetgeo.2020.104829.
- RANGEL HD & MARTINS CC. 1998. Principais compartimentos exploratórios, Bacia de Campos. In: TAHA M. *Searching for Oil and Gas in the Land of Giants*. Rio de Janeiro, RJ, Brazil, Schlumberger p. 32–40.
- ROSS CP & KINMAN DL. 1995. Nonbright-spot AVO: two examples. *Geophysics*, 60(5): 1398–1408. DOI: 10.1190/1.1443875.
- RUTHERFORD SR & WILLIAMS RH. 1989. Amplitude versus offset variation in gas sand. *Geophysics*, 54(6): 680–688. DOI: 10.1190/1.1442696.
- SIMM R, KEMPER M & DEO J. 2002. AVO Impedance: A new attribute for Fluid and Lithology Discrimination. In: *Petex Conference*. London.
- SIMM R & BACON M. 2014. *Seismic Amplitude: An Interpreter's Handbook*. Cambridge University Press, 279 pp.
- VEEKEN PCH & Da SILVA M. 2004. Seismic Inversion Methods and Some of their Constraints. *First Break*, 22(6): 15–38. DOI: 10.3997/1365-2397.2004011.
- VERNIK L. 2016. *Seismic petrophysics in quantitative interpretation*. Society of Exploration Geophysicists, Tulsa, USA. 226 pp.
- WHITCOMBE DN, CONNOLLY PA, REAGAN RL & REDSHAW TC. 2002. Extended elastic impedance for fluid and lithology prediction. *Geophysics*, 67(1): 63–67. DOI: 10.1190/1.1451337.
- WHITE RE & SIMM RW. 2003. Tutorial – good practice in well ties. *First Break*, 21(10): 75–83. DOI: 10.3997/1365-2397.21.10.25640.

M.P.: Conceptualization, Methodology, Software, Validation, Investigation, Writing – original draft, Writing – review & editing, Visualization. **W.M.L.:** Conceptualization, Methodology, Validation, Resources, Investigation, Writing – original draft, Writing – review & editing, Supervision.

Received on December 8, 2021 / Accepted on April 12, 2022